Self-Shielding Magnetized vs. Shaped Parallel-Magnetized PM Brushless AC Motors

Y. Pang*, Z. Q. Zhu* and D. Howe*

Abstract - The performance of two designs of permanent magnet brushless motor, by having self-shielding magnetized magnets or sinusoidally shaped parallel-magnetized magnets with essentially sinusoidal airgap flux distributions, are compared. It is shown that the parallel-magnetized motor with shaped sintered NdFeB magnets can result in a higher airgap flux density and torque density than that of a self-shielding magnetized motor equipped with an anisotropic injection moulded NdFeB ring magnet.

Keywords: brushless ac, electrical motor, magnetization, magnet shaping, permanent magnet, self-shielding.

1. Introduction

Asinusoidal back-emf waveform is desirable for brushless ac motors in order to eliminate excitation torque ripple. This can be achieved by employing skew and/or a distributed winding and/or shaping the magnets [1]. In general, however, a sinusoidal airgap field distribution is preferred, since it reduces the stator iron loss and the cogging torque, while a concentrated winding has a shorter end-winding, which is conducive to a low copper loss and high efficiency. A sinusoidal airgap field distribution may be achieved by shaping the magnets [2] or employing self-shielding magnetization [3-5].

This paper presents a comparative study of the design and performance of two BLAC motors, one employing optimally shaped, parallel-magnetized sintered anisotropic NdFeB magnets and the other employing an injection moulded anisotropic NdFeB magnet, which was oriented in a self-shielding powder aligning field and subsequently impulse magnetized with a self-shielding field distribution [6]. The design of both motors will be described, and their performance, in terms of their airgap field distribution, back-emf waveforms, cogging torque, copper loss, torque density, and efficiency, will be compared.

The design of the self-shielding magnetized motor is optimized for maximum efficiency, and is used as a benchmark against which the other motor, whose magnets have a sinusoidal profile in order to obtain a sinusoidal airgap flux density distribution, is compared. Comparisons are made when both motors are designed to have either the same outer dimension or the same output torque, and have the same copper loss. It will be shown that the motor with shaped parallel-magnetized sintered NdFeB magnets has a higher airgap flux density and torque density than the self-shielding magnetized motor with anisotropic bonded NdFeB magnets. Finally, it will be discussed that when the self-shielding magnetized sintered anisotropic NdFeB magnet ring can be developed in the future, the self-shielding magnetized motor may have its advantages over shaped parallel-magnetized motor in terms of the airgap flux density.

This paper was received the best paper award from ICEMS 2004, which held in Jeju Island, Korea from Oct. 31 to Nov. 3, 2004

* Department of Electronic & Electrical Engineering, University of Sheffield, Mappin Street, Sheffield S1 3JD, UK(Z.Q.Zhu@sheffield.ac.uk)

Received June 26, 2004 ; Accepted January 27, 2005

2. Self-Shielding Magnetized Motor

A 3-phase, 12-pole, 18-slot self-shielding magnetized motor with a self-shielding magnetized anisotropic injection moulded NdFeB ring magnet and a non-overlapping stator winding is shown in Fig. 1. The specifications and parameters are given in Table I. The remanence of the magnet B_r=0.6T, and the peak airgap flux density B_{gmax}=0.64T. The split ratio, i.e. a ratio of rotor to stator diameter, is optimized for maximum efficiency.

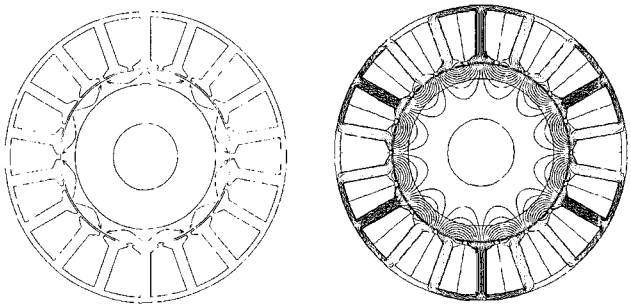

(a) Cross-section (b) Open circuit flux distribution

Fig. 1 3-phase, 12-pole, 18-slot self-shielding magnetized motor.

Table 1 Specification and Parameters of Self-Shielding Magnetized Motor

Rated torque, T_N	2.4 Nm
Rated speed, n	400 rpm
Pole-pair number, p	6
Slot number, N_s	18
Stator outer radius, R_{so}	45 mm
Stator bore radius, R_{si}	27.5 mm
Axial length, l_a	52 mm
Airgap length, g	0.5 mm
Winding turn per phase, N_w	78
Peak phase current, I_p	12.5 A
Copper loss, P_{cu}	43.1 W

For an internal rotor slotless self-shielding magnetized motor with ideal sinusoidal magnetization, assuming a unity relative permeability of the magnet, the airgap flux density on the stator bore can be calculated by [7]:

$$B_g = B_{gm}\cos p\theta = 2B_r \frac{p}{1+p}\frac{1}{K}\left(\frac{R_m}{R_{si}}\right)^{p+1}\left[1-\left(\frac{R_r}{R_m}\right)^{p+1}\right]\cos p\theta \quad (1)$$

$$K = \begin{cases} 1-\left(\dfrac{R_r}{R_{si}}\right)^{2p} & \text{for iron-cored Halbach motor} \\ 1 & \text{for air-cored Halbach motor} \end{cases} \quad (2)$$

where B_{gm} is the maximum value of airgap flux density, B_r is the remanence of permanent magnet, p is the number of pole-pairs, R_m is the outer radius of rotor magnet, R_{si} is the inner radius of stator, R_r is the inner radius of rotor magnet, θ is the mechanical angle.

The corresponding phase back-emf waveform can be calculated by:

$$E_{ph} = 2B_{gm}N_w l_a \frac{\omega_{elec}}{p} R_{si} K_{dp} \sin(\omega_{elec} t) \quad (3)$$

$$K_{dp} = \begin{cases} \dfrac{\sqrt{3}}{2} & \text{for } 120^o \text{ winding pitch} \\ 1 & \text{for } 180^o \text{ winding pitch} \end{cases} \quad (4)$$

where ω_{elec} is the electrical angular speed, N_w is the number of turns of phase winding, l_a is the axial length of lamination.

However, due to stator slotting, magnetic saturation, and non-ideal magnetization, the airgap field distribution may be non-sinusoidal. In this case, it can be expressed as:

$$B_g = \sum_{i=1,3,5...} B_{gmi}\cos(ip\theta) \quad (5)$$

where B_{gmi} is the peak value of i[th] harmonic of airgap flux density and can be determined from the Fourier series analysis of airgap field distribution which is obtained from finite element analysis. The equation of phase back-emf is then modified as:

$$E_{ph} = 2N_w l_a \frac{\omega_{elec}}{p} R_{si} \sum_{i=1,3,5...} B_{gmi} K_{dpi} \sin(i\omega_{elec} t) \quad (6)$$

$$K_{dpi} = \begin{cases} \sin\left(\dfrac{i\pi}{3}\right) & \text{for } 120^o \text{ winding pitch} \\ 1 & \text{for } 180^o \text{ winding pitch} \end{cases} \quad (7)$$

Fig. 2 shows the analytically and finite element predicted airgap field distribution and back-emf waveform in both iron-cored and air-cored self-shielding magnetized motors, in which the same stator is employed. The calculated results show that the airgap field distributions are essentially sinusoidal, albeit being modulation by the stator slotting. It can also be seen that iron-cored self-shielding magnetization results in higher airgap flux density, and consequently its phase back-emf waveform becomes non-sinusoidal due to magnetic saturation of tooth body.

Fig. 3 shows the finite element predicted cogging torque waveforms of both iron-cored and air-cored self-shielding magnetized motor. It can be seen that for iron-cored and air-cored self-shielding magnetized motors, their cogging torques are ~3% and ~1% of the rated torque, respectively.

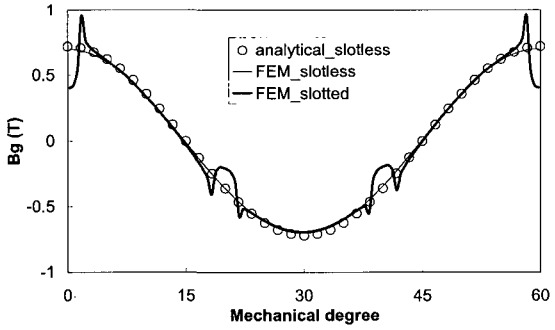

(a) Airgap field (iron cored)

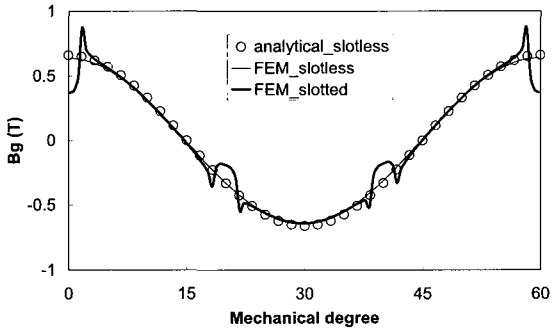

(b) Airgap field (air cored)

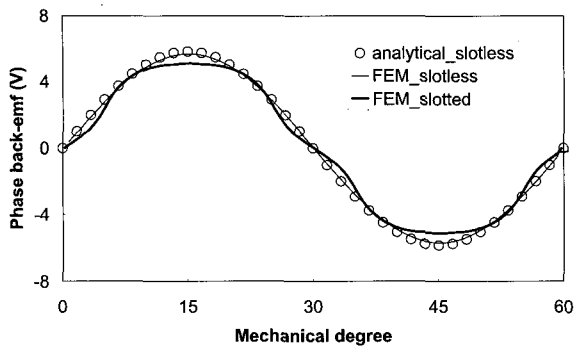

(c) Phase back-emf @ 400rpm (iron cored)

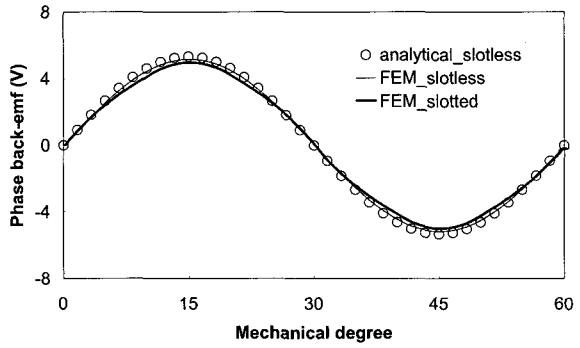

(d) Phase back-emf @ 400rpm (air cored)

Fig. 2 Analytical and finite element prediction of self-shielding magnetized motor.

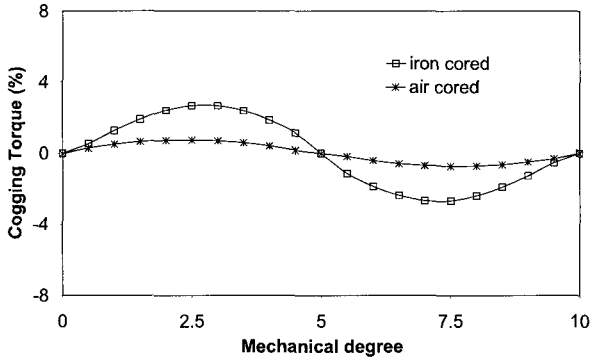

Fig. 3 Finite element predicted cogging torque for self-shielding magnetized motor.

3. Parallel-Magnetized Motor

It is assumed that the magnets are parallel-magnetized sintered NdFeB with a remanence B_r=1.2T and a maximum radial thickness of 3mm, as illustrated in Fig. 4, their outer surface being shaped according to (8). The influence of Δm has been investigated in order to derive the most appropriate magnet shape.

$$\Delta h = \Delta m \cos(p\theta) \tag{8}$$

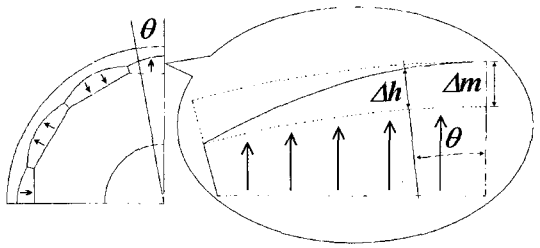

Fig. 4 Sinusoidally shaped magnet.

Initially, the motor was designed to have the same airgap flux density distribution as the self-shielding magnetized motor, so that the same stator lamination could be used. However, since the magnet has a higher remanence, the airgap length had to be increased from 0.5mm to 2mm in order to achieve the same maximum airgap flux density, as shown in Fig. 5.

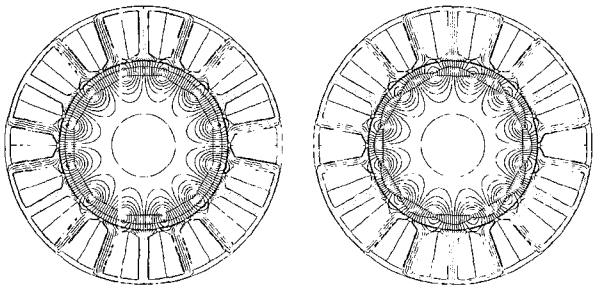

(a) Without shaping (b) With shaping

Fig. 5 Field distribution of slotted parallel-magnetized motor with/without sinusoidal magnet shaping.

From a series of finite element analyses, it was found that a perfect sinusoidal airgap flux distribution could be achieved with Δm=1.5mm.

Based on the airgap field analytical model in [8], the airgap field distribution of parallel-magnetized motor can be estimated by:

$$B_g = \sum_{n=1,3,5...}^{\infty} K_B(n) f_B(R_{si}) \cos(np\theta) \tag{9}$$

$$\text{where } f_B(R_{si}) = 2\left(\frac{R_m}{R_{si}}\right)^{np+1} \tag{10}$$

$$K_B(n) = \frac{\mu_0 M_n np}{(np)^2 - 1} \frac{(A_{3n}-1) + 2\left(\frac{R_r}{R_m}\right)^{np+1} - (A_{3n}+1)\left(\frac{R_r}{R_m}\right)^{2np}}{2\left[1-\left(\frac{R_r}{R_{si}}\right)^{2np}\right]} \tag{11}$$

$$A_{1n} = \frac{\sin\left[(np+1)\frac{\pi}{2p}\right]}{(np+1)\frac{\pi}{2p}} \tag{12}$$

$$A_{2n} = \frac{\sin\left[(np-1)\frac{\pi}{2p}\right]}{(np-1)\frac{\pi}{2p}} \tag{13}$$

$$A_{3n} = \left(np - \frac{1}{np}\right)\frac{M_{rn}}{M_n} + \frac{1}{np} \tag{14}$$

$$M_{rn} = \frac{B_r}{\mu_0}(A_{1n} + A_{2n}) \tag{15}$$

$$M_{tn} = \frac{B_r}{\mu_0}(A_{1n} - A_{2n}) \tag{16}$$

$$M_n = M_{rn} + npM_{tn} \tag{17}$$

Although (9) is developed for machines having uniform radial magnet thickness, it is reasonable to use (9) to estimate the airgap field distribution in the parallel-magnetized magnet motor having flat-bottom permanent magnet, Fig. 5, when the number of pole-pairs is relatively high.

For the optimal sinusoidally shaped parallel-magnetized motor as shown in Fig. 5(b), it is assumed that the airgap field distribution is sinusoidal and its peak value is equal to that in the original parallel-magnetized motor shown in Fig. 5(a), i.e.

$$B_{g\,max} = \sum_{n=1,3,5...}^{\infty} K_B(n) f_B(R_{si}) \tag{18}$$

Analytically calculated airgap field distribution and phase back-emf waveform are shown in Fig. 6, together with finite element calculated results. It confirms that by employing optimally shaped magnets a sinusoidal back-emf waveform can be achieved, while the cogging torque is reduced from 8% to ~1%, as shown in Fig. 7.

Although the airgap flux density in a self-shielding magnetized magnet motor could be increased by employing sintered NdFeB segments, more than 3 magnet segments per pole are required in order to obtain approximately sinusoidal airgap flux distribution, otherwise the performance will be deteriorated [9]. In contrast, only one parallel-magnetized magnet per pole is required and this can be impulse magnetized in a simple magnetizing fixture.

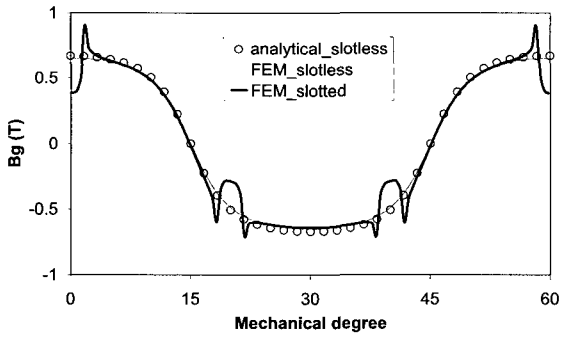

(a) Airgap field distribution (without shaping)

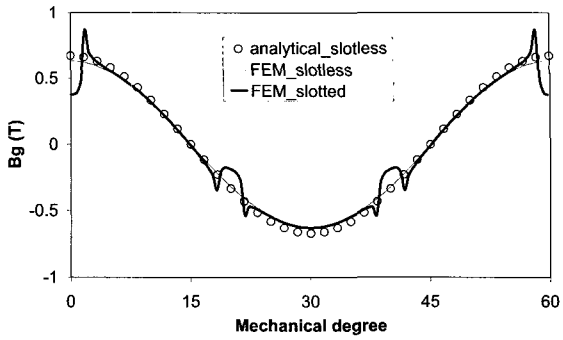

(b) Airgap field distribution (with shaping)

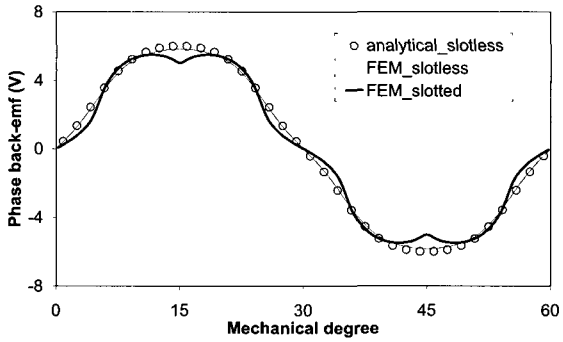

(c) Phase back-emf @ 400rpm (without shaping)

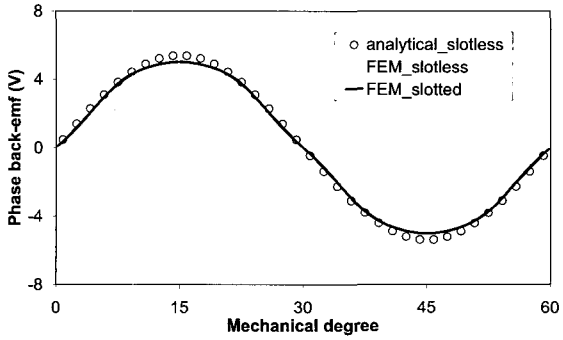

(d) Phase back-emf @ 400rpm (with shaping)

Fig. 6 Analytical and finite element prediction of parallel-magnetized motor.

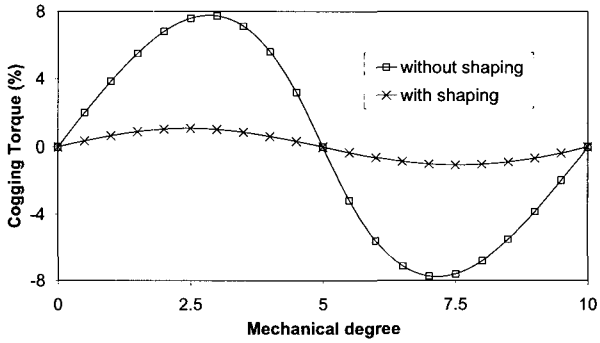

Fig. 7 Finite element predicted cogging torque of parallel-magnetized motor.

In the following section, the performance of the self-shielding and parallel-magnetized magnet machines are compared when they have the same airgap length.

4. Comparison of Self-Shielding Magnetized and Parallel-magnetized Motors

Three parallel-magnetized motors were designed to quantify the performance improvement, which can be achieved by using sinusoidally shaped magnets. The motors have the same axial length (52mm), airgap length (0.5mm) and the magnet thickness (3mm), as the self-shielding magnetized motor, which was described in Section II. Consequently, a higher airgap flux density (B_{gmax}=1.0T) is achieved. The rotor magnets are shaped to achieve a sinusoidal airgap flux density distribution, as described in the proceeding section, while the stator laminations and the windings are re-designed to maintain the same maximum flux density in the stator lamination.

4.1 Motor with Same Outer Diameter and Output Torque as Self-shielding Magnetized Motor

This magnetized motor, designated M1, was designed to have the same outer diameter (90mm) and output torque as the self-shielding magnetized motor. Since the airgap flux density is increased from 0.64T to 1T, the split ratio was decreased, the optimal stator bore radius being reduced to 25.5mm, The tooth-width was increased from 3.4mm to 5mm in order to maintain the same peak core flux density, and the back-iron was similarly increased, as shown in Fig. 8.

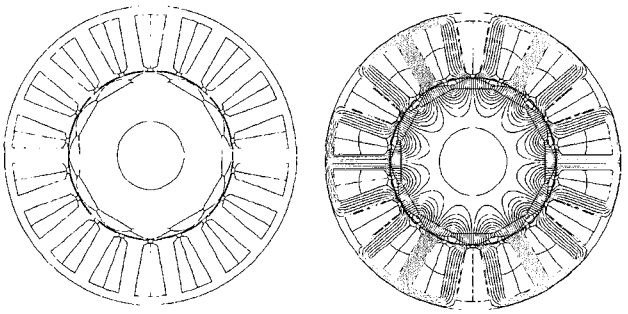

(a) Cross-section (b) Field distribution

Fig. 8 Parallel-magnetized motor M1.

The number of turns per phase was also reduced to 42. A sinusoidal airgap flux distribution was achieved again with Δm=1.5mm. Compared to the self-shielding magnetized motor, the copper loss is reduced by >40% and the efficiency increased by 10%, due to the increase of airgap flux density, Fig. 9. It should be noted, however, that due to the low speed operation, the iron losses of both machines are relatively low, being only ~6% of the copper loss for the self-shielding magnetized motor and ~10% of the copper loss for motor M1.

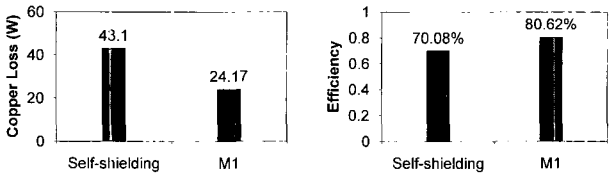

(a) Copper loss (b) Efficiency

Fig. 9 Performance of M1.

4.2 Motor with the Same Outer Diameter and Copper Loss as Self-shielding Magnetized Motor

Neglecting the variation in iron loss and maintaining the same thermal performance, thus the motor, designated M2, was designed to have the same outer diameter and copper loss as the self-shielding magnetized motor. Thus, M2 is identical to M1, except that the amplitude of the phase current is increased from 15.8A to 21.1A. Compared to the self-shielding magnetized motor, the output torque is increased by 30% and the efficiency is improved from 70.08% to 75.72%, Fig. 10.

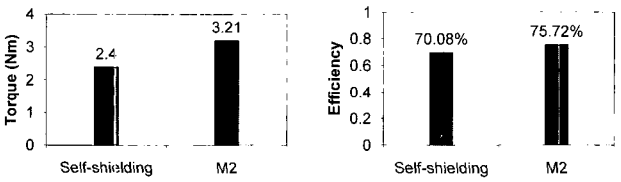

(a) Output torque (b) Efficiency

Fig. 10 Performance of M2.

4.3 Motor with the Same Output Torque and Copper Loss as Self-shielding Magnetized Motor

This motor, designated M3, was designed to have the same output torque and copper loss as the self-shielding magnetized motor. Hence, both motors have the same efficiency. However, for simplicity, the change in thermal dissipation which results due to the reduction in the outer diameter was neglected. Therefore, the outer diameter of motor M3 was reduced to 77.5mm, the corresponding optimal stator bore diameter being 44mm, whilst the number of turns per phase and the amplitude of the phase current are 54 and 14.3A, respectively. A sinusoidal airgap field distribution was again achieved with Δm=1.5mm, Fig. 11 Comparing to the self-shielding magnetized motor, the stator outer radius is reduced by ~10% whilst the torque density is increased by ~35%. As can be seen from Fig. 12, the torque density for motors M2 and M3 is similar. It will be noted that the optimal value of Δm for a sinusoidal airgap flux density distribution is the same for motors M1,

M2, and M3, primarily as a result of all the motors having the same airgap length and maximum magnet thickness.

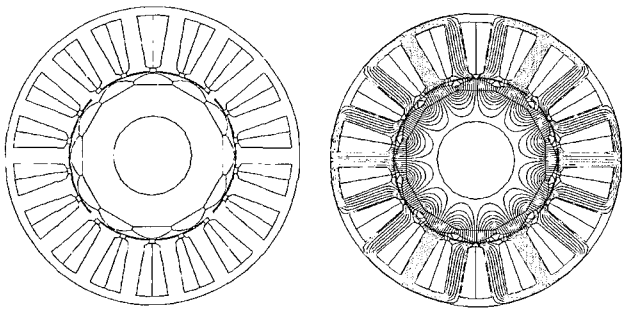

(a) Cross-section (b) Field distribution

Fig. 11 Parallel-magnetized motor M3.

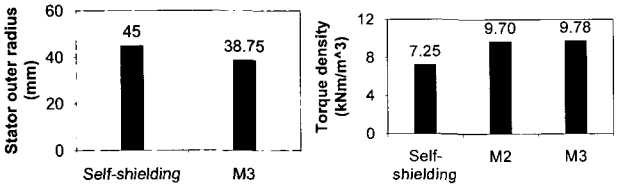

(a) Stator outer radius (b) Torque density

Fig. 12 Performance of M3.

5. Discussions

In the forgoing comparisons, a bonded anisotropic NdFeB magnet self-shielding ring, in which the magnet remanence is only 0.6T, is employed in the self-shielding magnetized motor. If the sintered anisotropic NdFeB magnet self-shielding magnetized ring can be developed in the future, the self-shielding motor may have its advantages over shaped parallel-magnetized motor in terms of the airgap flux density. Fig. 13 compares the corresponding ratio of the maximum airgap flux density in air-cored or iron-cored self-shielding magnetized motor to that in shaped parallel-magnetized motor when their magnet remanence and airgap length are identical, being 1.2T and 0.5mm, respectively.

It can be seen that the ratio of B_{gmax} of self-shielding magnetized motor to B_{gmax} of shaped parallel-magnetized motor can be improved by increasing either the number of pole-pairs or the ratio of magnet thickness to pole pitch, h_m/T_p. For air-cored self-shielding magnetized motor, when h_m/T_p is higher than 0.2, its maximum airgap flux density can be higher than that of parallel-magnetized motor. The airgap flux density in self-shielding magnetized motor can be significantly enhanced by employing the back-iron, especially when the magnet is thin. When the number of pole-pairs p=1, the iron-cored self-shielding magnetized motor and the shaped parallel-magnetized motor become the same motor and hence have the same airgap maximum flux density. When the number of pole-pairs is higher than 1, the maximum airgap flux density of iron-cored self-shielding magnetized motor is always higher than that of parallel-magnetized motor.

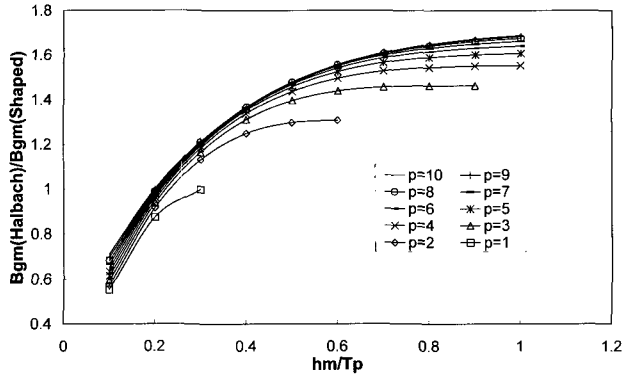

(a) Air-cored self-shielding magnetized motor and shaped parallel-magnetized motor

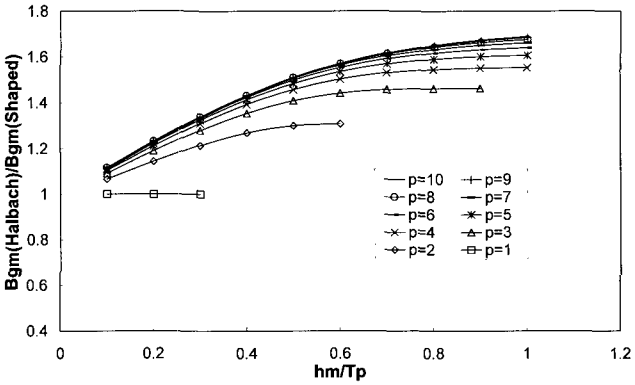

(b) Iron-cored self-shielding magnetized motor and shaped parallel-magnetized motor

Fig. 13 Variation of ratio of maximum flux densities in self-shielding magnetized motor and shaped parallel-magnetized motor with ratio of magnet thickness to pole pitch for different number of pole-pairs (B_r=1.2T, g=0.5mm, R_{so}=45mm, R_{si}= 27.5mm).

6. Conclusions

A self-shielding magnetized PM motor equipped with an anisotropic injection moulded NdFeB ring magnet and a parallel-magnetized PM motor equipped with sintered anisotropic magnets have been compared. It has been shown that a sinusoidal airgap flux distribution can be obtained in both types of motor. Thus, their back-emf waveforms are essentially sinusoidal and they have negligible cogging torque. However, a motor with shaped sintered NdFeB magnets results in a higher airgap flux density and a higher torque density than the self-shielding magnetized motor, although in the future when the sintered

anisotropic NdFeB magnet self-shielding magnetized ring is developed, the self-shielding motor may have its advantages over shaped parallel-magnetized motor in terms of the airgap flux density.

References

[1] T. M. Jahns, and W. L. Soong, "Pulsating torque minimization techniques for permanent magnet AC motor drives – a review", *IEEE Transactions on Industrial Electronics,* Vol.43, No.2, pp.321-330, April. 1996.

[2] R. J. Strahan, and D. B. Watson, "Effects of airgap and magnet shapes on permanent magnet reluctance torque", *IEEE Transactions on Magnetics,* Vol.35, No.1, pp.536-542, January. 1999.

[3] J.C. Mallinson, "One-sided fluxes – a magnetic curiosity?", *IEEE Transactions on Magnetics*, Vol.9, No.4, pp.678-682, December. 1973.

[4] K. Halbach, "Design of permanent magnet multipole magnets with oriented rare earth cobalt material" , *Nuclear Instruments & Methods*, vol.169, pp.1-10, 1980.

[5] Z. Q. Zhu, and D. Howe, "Halbach permanent magnet machines and applications: a review", *IEE Proceedings of Electrical Power Applications,* Vol.148, No.4, pp.299-308, July. 2001.

[6] Z. Q. Zhu, Z. P. Xia, K. Atallah, G. W. Jewell, and D. Howe, "Powder alignment system for anisotropic bonded NdFeB Halbach cylinders", *IEEE Transactions on Magnetics,* Vol.36, No.5, pp.3349-3352, September. 2000.

[7] Z. P. Xia, Z. Q. Zhu, and D. Howe, "Analytical magnetic field analysis of Halbach magnetized permanent magnet machines", *IEEE Transactions on Magnetics*, vol.40, no.4, pp.1864-1872, July. 2004.

[8] Z. Q. Zhu, D. Howe, and C. C. Chan, "Improved analytical model for predictng the magnetic field distribution in brushless permanent-magnet machines", *IEEE Transactions on Magnetics*, Vol.38, No.1, pp.229-238, January. 2002.

[9] Z. Q. Zhu, Z. P. Xia, and D. Howe, "Comparison of Halbach magnetized brushless machines having discrete magnet segments or single ring magnet", *IEEE Transactions on Magnetics*, Vol.38, No.5, pp.2997-2999, September. 2002.

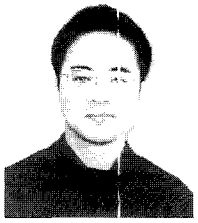

Y. Pang

He received the B.Eng and M.Sc. degrees in electrical engineering from Zhejiang University, Hangzhou, China, in 1997 and 2000, respectively. Currently, he is a PhD student at the University of Sheffield, Sheffield, UK, working on novel permanent magnet machines for electric vehicle application.

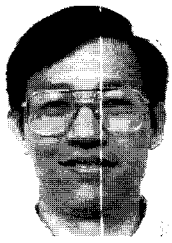

Z. Q. Zhu

He received the B.Eng. and M.Sc. degrees from Zhejiang University, Hangzhou, China, in 1982 and 1984, respectively, and was awarded the Ph.D. by the University of Sheffield, Sheffield, UK, in 1991, all in electrical and electronic engineering.

From 1984 to 1988 he lectured in the Department of Electrical Engineering at Zhejiang University. Since 1988, he has been with the University of Sheffield, where he is currently Professor of Electrical Engineering. His current major research interests include application, control, and design of permanent magnet machines and drives.

Tel: 44-114-2225195 Fax: 44-114-2225196

David Howe

He received the B.Tech and M.Sc. degrees from the University of Bradford, in 1966 and 1967, respectively, and a Ph.D. from the University of Southampton in 1974, all in electrical power engineering.

He has held academic posts at Brunel and Southampton Universities, and spent a period in industry with NEI Parsons Ltd working on electromagnetic problems related to turbo-generators. He is currently Professor of Electrical Engineering at the University of Sheffield, where he heads the Electrical Machines and Drives Research Group. His research activities span all facets of controlled electrical drive systems, with particular emphasis on permanent magnet excited machines.

Prof. Howe is a Chartered Engineer, a Fellow of the Royal Academy of Engineering, and a Fellow of the IEE, UK.